Speckle decorrelation in Ultrasound-modulated optical tomography made by heterodyne holography

M. Gross[1]

[1] *Laboratoire Charles Coulomb - UMR 5221 CNRS-UM2 Université Montpellier Place Eugène Bataillon 34095 Montpellier, France*

Ultrasound-modulated optical tomography (UOT) is a technique that images optical contrast deep inside scattering media. Heterodyne holography is a promising tool able to detect the UOT tagged photons with high efficiency. In this work, we describe theoretically the detection of the tagged photon in heterodyne holography based UOT, show how to filter the untagged photon discuss, and discuss the effect of speckle decorrelation. We show that optimal detection sensitivity can obtain, if the frame exposure time is of the order of the decorrelation time.

arXiv:1606.02902v1 [physics.optics] 9 Jun 2016

OCIS codes: 170.1650, 170.3660, 290.7050, 090.0090, 170.7050

Light scattering prevents optical imaging from achieving high resolution inside scattering media deeper than about 1 mm in tissue. Ultrasound-modulated optical tomography (UOT)[1, 2] also called acousto-optic imaging [3], has been developed to overcome this limit by combining ultrasonically defined spatial resolution and optical contrast (i.e. sensitivity to the bulk optical properties like absorption). One of the purpose of the technique is to use the optical contrast to detect breast tumors that cannot be seen with ultrasound, because the ultrasonic contrast is too low. In an UOT experiment, the light scattered through a diffusing sample crosses an ultrasonic beam, and, due to the acousto-optic effect, undergoes a frequency shift equal to the ultrasonic frequency [4, 5]. By detecting the frequency-shifted photons, called tagged photons, and by plotting their weight as a function of the ultrasonic beam geometry, 2D or 3D images of the sample can then be obtained with ultrasonic spatial resolution.

Various methods have been developed to detect the very low tagged photons signal out of a large background of untagged photons [2, 3]. First experiments use single-pixel detector and detection of the tagged photon AC modulation at the ultrasonic frequency [4, 6, 7]. Since each speckle grain oscillates with a different phase, the single pixel method detects, with a good efficiency, no more than one speckle grain. This severely limits the detection etendue (defined as the product of the detection area and the acceptance solid angle). To increase the detection etendue without reducing the modulation depth, three types of methods have been developed. The first type relies on incoherent detection with a narrow spectral filter (∼MHz) that filter out the untagged light. A large-area single-pixel detector can be used. Examples include Fabry-Perot interferometers [8–10] and spectral-hole burning [11–13] based methods. These techniques require bulky and expensive equipment. The second and third types of method use interferences and are thus sensitive to the signal phase decorrelation due to the living tissue inner motions, and to the corresponding Doppler broadening. For breast, this broadening is 1.5 kHz [14]. The second method is based on a photorefractive crystal, which records the volume hologram of the sample scattered field. This hologram can be then used to generate a diffracted field able to interfere with the scattered field on a large area single-pixel detector [15–18]. The method has a large optical etendue ($\sim 10^8$ speckle), but is somewhat sensitive to decorrelation, since the response time of the crystal is usually much longer than the speckle correlation. Promising results are expected with Sn2P2S6:Te and Nd:YVO4 crystals, because of their short response times [19, 20].

The third type of method uses a pixel array, i.e., a camera, to detect the UOT tagged photons [21–24]. The optical etendue ($\sim 10^5$ to 10^6 speckle) is then related to the number of pixels of the camera. The camera method has been improved by adapting the heterodyne holography technique [25] to the tagged photon detection [26]. By tuning the LO beam frequency near the ultrasonic sideband, and by using a properly adjusted spatial filter, the tagged photons were detected selectively. Moreover, optimal noise detection was obtained, since shot noise is the dominant noise in heterodyne holography [27–29]. The reference [26] experiment was nevertheless performed with a phantom sample, whose decorrelation is low, and it is generally considered that the heterodyne holography UOT method cannot be used with a living sample, whose speckle decorrelation time τ_c is shorter than the time needed to record four camera frames (where $\tau_c = 0.1$ ms for the light scattered "in vivo" through a woman's breast [14]). Resink et al. [3] wrote, for example, "all frames of the one to four phases [i.e. the four frames of the camera] should be taken within the speckle decorrelation time".

In this work, we analyzed theoretically the heterodyne holography UOT detection scheme, and we calculated how untagged photons, speckle noise, shot noise, decorrelation and etendue, affect the UOT signal. By adjusting the calculation parameter, we got results very similar to the ones of [26]. By comparing results obtained with and without decorrelation, we showed that the Resink et al. remark is not valid, and that heterodyne holography remains, with decorrelation, an optimal detection scheme of the tagged photons. Note that this point was already demonstrated for the detection of the untagged photon in experiments done without ultrasound [30–35].

To introduce our theoretical discussion, let us consider

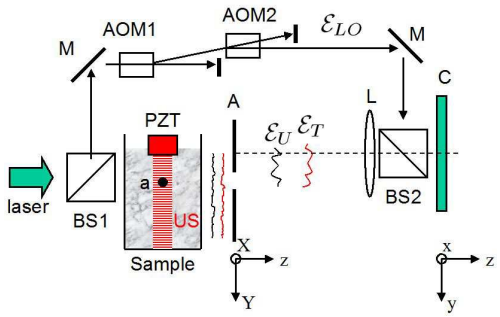

FIG. 1. Typical UOT setup: BS1, BS2: beam splitter; M: mirror; AOM1,AOM2: acousto optic modulator; PZT: piezoelectric transducer that generates the ultrasonic beam US; a: absorber embedded in the diffusing sample; A: rectangular aperture; L: lens of focal d; C: camera; $\mathcal{E}_{LO}, \mathcal{E}_T, \mathcal{E}_U$: LO, tagged and untagged fields.

a typical heterodyne holographic UOT setup (Fig. 1). A laser of frequency ω_L is split by the beam splitter BS1 into a signal beam and a local oscillator (LO) beam. The signal beam travels trough the diffusing sample S and is scattered by it. The sample is explored by an ultrasonic beam US of frequency ω_{US}. The light transmitted by the sample exhibit to components. The first component at $\omega_T = \omega_L + \omega_{US}$ is weak ($\sim 10^{-2}$ to 10^{-4} in power), and corresponds to the tagged photons that have interacted with the ultrasonic (US) beam. The second component at $\omega_U = \omega_L$ is the main one ($\simeq 100\%$ in power). It corresponds to untagged photons which have not interacted with US.

A rectangular aperture A, located off axis near the sample, control the size and location of the zone of the sample where of the tagged and untagged fields $\mathcal{E}_T$ and $\mathcal{E}_T$ are detected. The $\mathcal{E}_T$ and $\mathcal{E}_T$ fields are mixed with the LO field $\mathcal{E}_{LO}$ by the beam splitter BS2, and the camera C records a sequence of M frames I_m (with $m = 0...M-1$) corresponding to the interference pattern: $\mathcal{E}_T + \mathcal{E}_U + \mathcal{E}_{LO}$, I_m being recorded at time $t_m = m\Delta t$, where $\Delta t = 2\pi m/\omega_C$ is the pitch in time, and ω_C is the camera frame frequency. The hologram H_C of the aperture A (that is back illuminated by $\mathcal{E}_T$ and $\mathcal{E}_U$) is calculated, in the camera plane C, by combining frames I_m. The hologram H_A, in the aperture plane A, is then calculated from H_C. The signal of interest (tagged or untagged photon) is calculated from H_A.

To analyze theoretically the Fig.1 experiment, let us define, in plane A and C, the untagged, tagged and LO fields and their respective complex amplitudes, which are slow varying with time t:

$$\begin{aligned}
\mathcal{E}_{A,U}(X,Y,t) &= E_{A,U}(X,Y,t)\ e^{j\omega_L t} + \text{c.c.} \qquad (1)\\
\mathcal{E}_{A,T}(X,Y,t) &= E_{A,T}(X,Y,t)\ e^{j(\omega_L+\omega_{US})t} + \text{c.c.}\\
\mathcal{E}_{C,U}(x,y,t) &= E_{C,U}(x,y,t)\ e^{j\omega_L t} + \text{c.c.}\\
\mathcal{E}_{C,T}(x,y,t) &= E_{C,T}(x,y,t)\ e^{j(\omega_L+\omega_{US})t} + \text{c.c.}\\
\mathcal{E}_{C,LO}(x,y,t) &= E_{LO}\ e^{j\omega_{LO} t} + \text{c.c.}
\end{aligned}$$

where c.c. is the complex conjugate. Here, X, Y are the coordinates in plane A, and x, y in plane C. To simplify theory, we have considered here that E_{LO} do not depend on x, y and t. In plane A, the tagged and untagged photon fields are fully developed speckle. The complex fields $E_{A,T/U}(X,Y,t_m)$ are thus random Gaussian complex quantities uncorrelated from one pixel X, Y to any other X', Y'. The random amplitudes $E_{A,T/U}(X,Y,t_m)$ do not depend on t_m without decorrelation, and are uncorrelated from one frame (i.e. m) to the next (i.e. $m+1$) with decorrelation.

A lens L, which is located near the camera, and whose focal plane is close to plane A, collects the fields. Because of L, the tagged and untagged fields in planes C and A are related by a Fourier transform

$$E_{A,U/T}(X,Y) = \tilde{E}_{C,U/T}(k_x,k_y) = \text{FFT}(E_{C,U/T}(x,y))$$

where $(X,Y) = (k_x,k_y)\times|\text{CA}|/k$ with $k = 2\pi/\lambda$. To simplify calculations, the discrete Fourier transform (FFT) is made within a calculation grid that fits with the camera pixels in plane C. The pitch Δx of the discrete coordinates x, y is thus equal to the size of the pixel of the camera. Because of the FFT, the pitch ΔX in plane A is

$$\Delta X = 2\pi|\text{CA}|\ /(Nk\Delta x) \qquad (2)$$

where N is the number of pixels of the camera ($N = 1024$ typically). The detection etendue is thus $G = S_A S_D/|\text{CA}|^2 = N^2\lambda^2$, where $S_A = |N\Delta X|^2$ and $S_C = |N\Delta y|^2$ are the areas of the calculation grid in plane A and C. The number of modes or speckle grains that can be detected is thus equal to the number of pixels of the camera N^2.

The frame signal I_m correspond to the sum of the tagged, untagged and LO photons. To detect the tagged photons, ω_{LO} is made close to the tagged photon frequency $\omega_L + \omega_{US}$. The LO and the tagged photons thus interfere (and are summed in fields), while the untagged photons do not interfere (and are summed in intensities). We have thus:

$$\begin{aligned}
I_m(x,y) = &\left|E_{C,T}(x,y,t_m) + c^m E_{LO}\right|^2 \qquad (3)\\
&+ \left|E_{C,U}(x,y,t_m)\right|^2
\end{aligned}$$

where $c = e^{j(\omega_{LO}-\omega_{US}-\omega_L)\Delta t}$ is the LO versus tagged photon shift of phase. On the other hand, to detect the untagged photons, ω_{LO} is close to ω_L, and I_m is given by an equation similar to Eq. 3, where the indexes U and T are exchanged, and where $c = e^{j(\omega_{LO}-\omega_L)\Delta t}$. Because of the random nature of light emission and camera photo conversion, the frame signal I_m is affected by shot noise yielding I'_m:

$$I'_m(x,y) = I_m(x,y) + s(x,y,m)\sqrt{I_m(x,y)}\ \ ) \qquad (4)$$

where the term $s\sqrt{I_m}$ accounts for shot noise. Here, I_m must be expressed in photo electron Units per pixel and per frame, while s is a real Gaussian random variable of

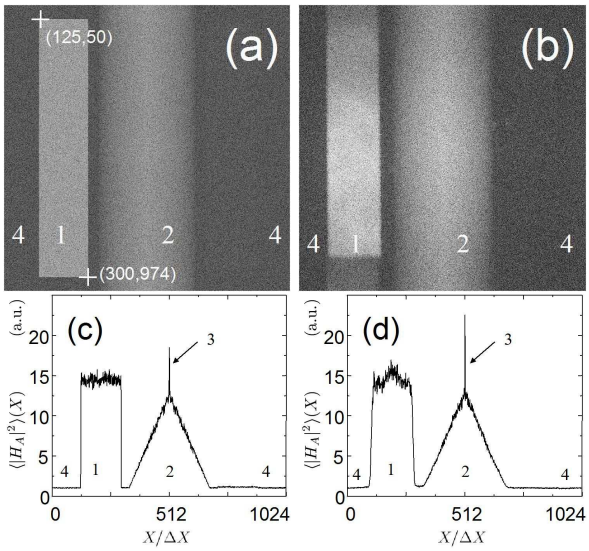

FIG. 2. Tagged intensity images $|H_A(X,Y)|^2$ (a,b) and curves $\langle|H_A(X)|^2\rangle$ (c,d) obtained by calculation (a,c) and from ref.[26] experiment (b,d). The images $|H_A(X,Y)|^2$ (a,b) are displayed in an arbitrary logarithmic scale. The curves $\langle|H_A(X)|^2\rangle$ (c,d) are normalized with respect to the background.

variance $\langle s^2\rangle = 1$ uncorrelated with pixels (i.e. X,Y) and with frames (i.e. m).

The hologram H_C is then calculated from I'_m. Without decorrelation, four phase detection of the tagged photons is made. We have thus: $H_C = \sum_{m=0}^{M} j^m I_m$ (where M frames is a multiple of four) and $\omega_{LO} = \omega_L + \omega_{US} + \omega_C/4$ yielding $c = j$ in Eq. 3. With decorrelation, two phase detection with two frames is made: $H_C = I_0 - I_1$, and $\omega_{LO} = \omega_L + \omega_{US} + \omega_C/2$ yielding $c = -1$. In H_C, the holographic term of interest: $E_{C,T}E^*_{LO}$ (where * is the complex conjugate operator), is proportional to the field $E_{C,T}$. Because of L, the holograms H_A and H_C in planes A and C are related by a Fourier transform

$$H_A(X,Y) = \tilde{H}_C(k_x,k_y) = \text{FFT}\ (\ H_C(x,y)\ ) \qquad (5)$$

We have calculated, without decorrelation, the tagged photon hologram H_A for $M = 12$ frames (like in [26]). The calculation is made with $|E_{LO}|^2 = 10^4$, $\langle|E_{A,T}|^2\rangle = 1.33$ and $\langle|E_{A,U}|^2\rangle = 3\times10^3$ photo electron per frame and per pixel, where $\langle\ \rangle$ is the average over X and Y within the aperture. Note that tagged and untagged energies ($\sum_{\text{pixels}}|E|^2$) are the same in planes A and C, because Eq.2 conserves energy. The coordinates of the upper left and bottom right aperture corners were $(125,50)$ and $(300,974)$.

We have displayed in Fig. 2 the arbitrary logarithmic scale intensity image $|H_A(X,Y)|^2$ obtained by calculation (a), and in experiment (b) [26]. Note that the calculation parameters were chosen here to fit with [26]. To further compare our calculation with [26], we have

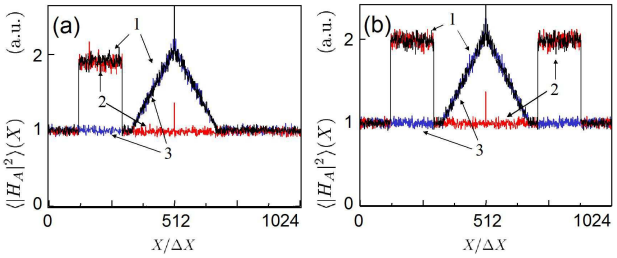

FIG. 3. Curves $\langle|H_A(X)|^2\rangle$ calculated without (a) and with decorrelation (b) by switching on and off the tagged and untagged photons signals.

calculated the curves $\langle|H_A(X)|^2\rangle$:

$$\langle|H_A(X)|^2\rangle = (1/N)\sum_X |H_A(X,Y)|^2 \qquad (6)$$

Figure 2 (c,d) show the curves $\langle|H_A(X)|^2\rangle$ obtained by calculation (c) and from [26] (d). The curves are normalized with respect to the background that is obtained without tagged and untagged photons and that corresponds to shot noise. The good agreement with [26] validates our theoretical calculation.

In figure 2, the tagged photon signal corresponds to the image of the aperture, i.e. to the bright rectangular zone 1, which is located in the left of images (a,b), because the aperture is located of axis. The aperture corresponds also to the rectangular walls 1, in curves (c,d). On the other hand, the blurred bright zone 2, in the center of (a,b), and the triangular wall 2, in (c,d), corresponds to a parasitic detection of the untagged photon signal, which does not cancel here because of decorrelation (in experiment) and shot noise (in experiment and calculation). The parasitic detection of the LO fields yields a very narrow peak located in the center of the calculation grid, which is only visible on the curves (arrow 3). To the end, shot noise yields a flat background in all points of the images and the curve (zones 4).

To confirm this analyse of Fig.2, and to evaluate how untagged photons, shot noise and decorrelation affect the UOT signal, we have calculated the curves $\langle|H_A(X)|^2\rangle$ without and with decorrelation by switching on and off the tagged and untagged photons. To better compare results obtained without and with decorrelation, the tagged and untagged photon energies were measured within a time equal to the recording time of the sequence of M frames ($2\pi M/\omega_C$) without decorrelation, and to the frame exposure time, which is made equal to τ_c, with decorrelation. Calculations were made with $|E_{LO}|^2 = 10^4$, $M\langle|E_{A,U}|^2\rangle = 10000$, $M\langle|E_{A,T}|^2\rangle = 1$ and $M = 12$ without decorrelation, and with $|E_{LO}|^2 = 10^4$, $\langle|E_{A,U}|^2\rangle = 250$ and $\langle|E_{A,T}|^2\rangle = 1$ with decorrelation. Note that the calculations are made with the same tagged photon signal with and without decorrelation (1 photo electron per pixel).

Figure 3 shows the curves obtained without (a) and

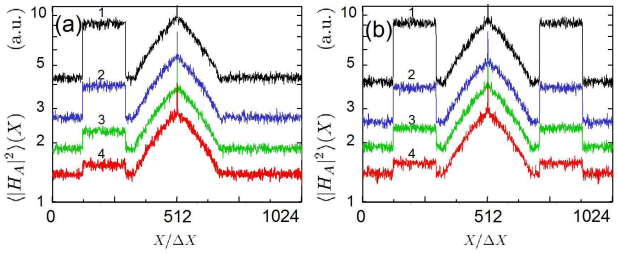

FIG. 4. Curves $\langle|H_A(X)|^2\rangle$ obtained without (a) and with decorrelation (b). Calculation is made with $\alpha = 1$ (1), 0.5 (2), 0.25 (3) and 0.125 (4). Plots are made in arbitrary logarithmic scale.

with (b) decorrelation. Curves 1 (back) were obtained with tagged and untagged photons, curves 2 (red) with tagged (and without untagged) photons, and curves 3 (blue) with untagged (and without tagged) photons. As seen, the rectangular walls (located on the left side of Fig.3(a) and on the left and right sides of Fig.3(b)) correspond to the tagged photon signal. On the hand, the triangular walls (located in the center of Fig.3(a) and (b)) correspond to the untagged photons. Note that the width of triangular walls is twice the width of the rectangular walls, which is itself proportional to the width of the aperture. By a proper choice of the aperture size, here and in [26], the rectangular and triangular walls are well separated, making possible to filter off the unwanted untagged photon signal. Note that the effect of the untagged photons is much lower without decorrelation. To still visualize them in Fig.3(a), we have performed the calculation with a much larger unttagged signal without decorrelation ($\langle|E_{A,U}|^2\rangle = 10^4$), than with decorrelation ($\langle|E_{A,U}|^2\rangle = 250$).

To evaluate tagged photon detection sensitivity limits, we have calculated $\langle|H_A|^2\rangle(X)$ curves by varying the total tagged photon energy per τ_c. The curves are plotted on Fig.4 with decorrelation (a) and without (b). Calculations were made with $|E_{LO}|^2 = 10^4$, $M\langle|E_{A,U}|^2\rangle = 10000$, $M\langle|E_{A,T}|^2\rangle = \alpha$ and $M = 12$ without decorrelation, and with $|E_{LO}|^2 = 10^4$, $\langle|E_{A,U}|^2\rangle = 250$ and $\langle|E_{A,T}|^2\rangle = \alpha$ with decorrelation, where α is the number of tagged photons per pixel with $\alpha = 1$, 0.5, 0.25, 0.125 and 0.0625 for curves 1 to 5. To better visualize them, the curves were plotted in log scale, and the curves were arbitrarily shifted up or down to better separate them from each other. The results of Fig.4 show that heterodyne holography UOT exhibits roughly the same sensitivity for the detection of the tagged photon with and without decorrelation. The key parameter is the tagged photon energy per pixel during the coherent measurement time with is equal to τ_c with decorrelation, and to time $M2\pi/\omega_C$ needed to record the sequence of M frames without decorrelation. A signal versus background ratio of 1 corresponds, with and without decorrelation, to one photo electron per pixel. By averaging over the about 10^5 pixels of the rectangular aperture, the sensitivity limit is improved down to about $1/\sqrt{10^5} \sim 1/300$ photo electron. This result agrees with what observed experimentally for the detection of the untagged photons [14].

In this letter, we have proposed a theoretical model to describe the detection of the tagged photons in heterodyne holography UOT. This model, which agrees with the results of [26], has been used to calculate how untagged photons, speckle noise, shot noise, decorrelation and etendue, affect the UOT signal. For a given coherent measurement time, which is $M2\pi/\omega_C$ and τ_c without and with decorrelation, the model yields the same detection sensitivity, and the same noise floor (one photon electron per pixel). Heterodyne holography UOT is thus shot noise limited. By averaging over the $K \sim 10^5$ pixels of the image of the aperture, the detection sensitivity becomes $1/\sqrt{K}$ photo electron per speckle (i.e per etendue λ^2). We hope this work will stimulate further UOT development.

This work has been carried out thanks to the supports of the LabEx NUMEV project (n° ANR-10-LABX-20) funded by the "Investissements d'Avenir" French Government program, managed by the French National Research Agency (ANR) and thanks to the ANR grand (reference n°ANR-11-BS04-0017: ICLM).

[1] Lihong Wang and Xuemei Zhao. Ultrasound-modulated optical tomography of absorbing objects buried in dense tissue-simulating turbid media. *Applied optics*, 36(28):7277–7282, 1997.

[2] Daniel S Elson, Rui Li, Christopher Dunsby, Robert Eckersley, and Meng-Xing Tang. Ultrasound-mediated optical tomography: a review of current methods. *Interface Focus*, 1(4):632–648, 2011.

[3] Steffen G Resink, Albert C Boccara, and Wiendelt Steenbergen. State-of-the art of acousto-optic sensing and imaging of turbid media. *Journal of biomedical optics*, 17(4):0409011–04090110, 2012.

[4] W Leutz and Georg Maret. Ultrasonic modulation of multiply scattered light. *Physica B: Condensed Matter*, 204(1):14–19, 1995.

[5] Lihong V Wang. Mechanisms of ultrasonic modulation of multiply scattered coherent light: an analytic model. *Physical Review Letters*, 87(4):043903, 2001.

[6] Lihong Wang, Steven L Jacques, and Xuemei Zhao. Continuous-wave ultrasonic modulation of scattered laser light to image objects in turbid media. *Optics letters*, 20(6):629–631, 1995.

[7] M Kempe, M Larionov, D Zaslavsky, and AZ Genack. Acousto-optic tomography with multiply scattered light. *JOSA A*, 14(5):1151–1158, 1997.

[8] Sava Sakadžić and Lihong V Wang. High-resolution ultrasound-modulated optical tomography in biological tissues. *Optics letters*, 29(23):2770–2772, 2004.

[9] Sri-Rajasekhar Kothapalli and Lihong V Wang. Ultrasound-modulated optical microscopy. *Journal of biomedical optics*, 13(5):054046–054046, 2008.

[10] Guy Rousseau, Alain Blouin, and Jean-Pierre Monchalin. Ultrasound-modulated optical imaging using a high-power pulsed laser and a double-pass confocal fabry–perot interferometer. *Optics letters*, 34(21):3445–3447, 2009.

[11] Youzhi Li, Philip Hemmer, Chulhong Kim, Huiliang Zhang, and Lihong V Wang. Detection of ultrasound-modulated diffuse photons using spectral-hole burning. *Optics express*, 16(19):14862–14874, 2008.

[12] Youzhi Li, Huiliang Zhang, Chulhong Kim, Kelvin H Wagner, Philip Hemmer, and Lihong V Wang. Pulsed ultrasound-modulated optical tomography using spectral-hole burning as a narrowband spectral filter. *Applied physics letters*, 93(1):011111, 2008.

[13] Huiliang Zhang, Mahmood Sabooni, Lars Rippe, Chulhong Kim, Stefan Kröll, Lihong V Wang, and Philip R Hemmer. Slow light for deep tissue imaging with ultrasound modulation. *Applied physics letters*, 100(13):131102, 2012.

[14] M Gross, P Goy, BC Forget, M Atlan, F Ramaz, AC Boccara, and AK Dunn. Heterodyne detection of multiply scattered monochromatic light with a multipixel detector. *Optics letters*, 30(11):1357–1359, 2005.

[15] Todd W Murray, Lei Sui, Gopi Maguluri, Ronald A Roy, Alex Nieva, Florian Blonigen, and Charles A DiMarzio. Detection of ultrasound-modulated photons in diffuse media using the photorefractive effect. *Optics letters*, 29(21):2509–2511, 2004.

[16] François Ramaz, B Forget, Michael Atlan, Albert-Claude Boccara, Michel Gross, Philippe Delaye, and Gérald Roosen. Photorefractive detection of tagged photons in ultrasound modulated optical tomography of thick biological tissues. *Optics express*, 12(22):5469–5474, 2004.

[17] Michel Gross, François Ramaz, B Forget, Michael Atlan, A Boccara, Philippe Delaye, and Gérald Roosen. Theoretical description of the photorefractive detection of the ultrasound modulated photons in scattering media. *Optics Express*, 13(18):7097–7112, 2005.

[18] Puxiang Lai, Xiao Xu, and Lihong V Wang. Ultrasound-modulated optical tomography at new depth. *Journal of biomedical optics*, 17(6):0660061–0660066, 2012.

[19] Salma Farahi, Germano Montemezzani, Alexander A Grabar, Jean-Pierre Huignard, and François Ramaz. Photorefractive acousto-optic imaging in thick scattering media at 790 nm with a sn 2 p 2 s 6: Te crystal. *Optics letters*, 35(11):1798–1800, 2010.

[20] B Jayet, JP Huignard, and F Ramaz. Fast wavefront adaptive holography in nd: Yvo 4 for ultrasound optical tomography imaging. *Optics express*, 22(17):20622–20633, 2014.

[21] S Leveque, AC Boccara, M Lebec, and H Saint-Jalmes. Ultrasonic tagging of photon paths in scattering media:? parallel speckle modulation processing. *Optics letters*, 24(3):181–183, 1999.

[22] Gang Yao, Shuliang Jiao, and Lihong V Wang. Frequency-swept ultrasound-modulated optical tomography in biological tissue by use of parallel detection. *Optics letters*, 25(10):734–736, 2000.

[23] Jun Li and Lihong V Wang. Methods for parallel-detection-based ultrasound-modulated optical tomography. *Applied optics*, 41(10):2079–2084, 2002.

[24] Jun Li, Geng Ku, and Lihong V Wang. Ultrasound-modulated optical tomography of biological tissue by use of contrast of laser speckles. *Applied optics*, 41(28):6030–6035, 2002.

[25] Frédérique Le Clerc, Laurent Collot, and Michel Gross. Numerical heterodyne holography with two-dimensional photodetector arrays. *Optics letters*, 25(10):716–718, 2000.

[26] Michel Gross, Philippe Goy, and Mohamed Al-Koussa. Shot-noise detection of ultrasound-tagged photons in ultrasound-modulated optical imaging. *Optics letters*, 28(24):2482–2484, 2003.

[27] Michel Gross and Michael Atlan. Digital holography with ultimate sensitivity. *Optics letters*, 32(8):909–911, 2007.

[28] Frédéric Verpillat, Fadwa Joud, Michael Atlan, and Michel Gross. Digital holography at shot noise level. *Display Technology, Journal of*, 6(10):455–464, 2010.

[29] Max Lesaffre, Nicolas Verrier, and Michel Gross. Noise and signal scaling factors in digital holography in weak illumination: relationship with shot noise. *Applied optics*, 52(1):A81–A91, 2013.

[30] Michael Atlan, Michel Gross, Benoit C Forget, Tania Vitalis, Armelle Rancillac, and Andrew K Dunn. Frequency-domain wide-field laser doppler in vivo imaging. *Optics letters*, 31(18):2762–2764, 2006.

[31] Michael Atlan and Michel Gross. Laser doppler imaging, revisited. *Review of Scientific Instruments*, 77(11):116103, 2006.

[32] Max Lesaffre, Michael Atlan, and Michel Gross. Effect of the photon's brownian doppler shift on the weak-localization coherent-backscattering cone. *Physical review letters*, 97(3):033901, 2006.

[33] Michael Atlan, Benoit C Forget, Albert C Boccara, Tania Vitalis, Armelle Rancillac, Andrew K Dunn, and Michel Gross. Cortical blood flow assessment with frequency-domain laser doppler microscopy. *Journal of biomedical optics*, 12(2):024019–024019, 2007.

[34] Michael Atlan and Michel Gross. Spatiotemporal heterodyne detection. *JOSA A*, 24(9):2701–2709, 2007.

[35] Michael Atlan, Michel Gross, Tania Vitalis, Armelle Rancillac, Jean Rossier, and AC Boccara. High-speed wave-mixing laser doppler imaging in vivo. *Optics Letters*, 33(8):842–844, 2008.